LAWRENCE
LIVERMORE
NATIONAL
LABORATORY

LLNL-JRNL-557573

Longitudinal Emittance Growth Due to Nonlinear Space Charge Effect

Y. Y. Lau, S. S. Yu, J. J. Barnard, P. A. Seidl

May 14, 2012

Physical Review Special Topics -- Accelerators and Beams

Disclaimer

This document was prepared as an account of work sponsored by an agency of the United States government. Neither the United States government nor Lawrence Livermore National Security, LLC, nor any of their employees makes any warranty, expressed or implied, or assumes any legal liability or responsibility for the accuracy, completeness, or usefulness of any information, apparatus, product, or process disclosed, or represents that its use would not infringe privately owned rights. Reference herein to any specific commercial product, process, or service by trade name, trademark, manufacturer, or otherwise does not necessarily constitute or imply its endorsement, recommendation, or favoring by the United States government or Lawrence Livermore National Security, LLC. The views and opinions of authors expressed herein do not necessarily state or reflect those of the United States government or Lawrence Livermore National Security, LLC, and shall not be used for advertising or product endorsement purposes.

Longitudinal emittance growth due to non-linear space charge effect

Y.Y. Lau,[1] Simon S. Yu,[1,2] John J. Barnard,[3] and Peter A. Seidl[2]
[1)] *The Chinese University of Hong Kong, Hong Kong*
[2)] *Lawrence Berkeley National Laboratory, Berkeley, California, USA*
[3)] *Lawrence Livermore National Laboratory, Livermore, California, USA*

(Dated: 26 November 2011)

Emittance posts limits on the key requirements of final pulse length and spot size on target in heavy ion fusion drivers. In this paper, we show studies on the effect of non-linear space charge on longitudinal emittance growth in the drift compression section. We perform simulations, using the 3-D PIC code WARP, for a high current beam under conditions of bends and longitudinal compression. The linear growth rate for longitudinal emittance turns out to depend only on the peak line charge density, and is independent of pulse length, velocity tilt, and/or the pipe and beam size. This surprisingly simple result is confirmed by simulations and analytic calculations.

PACS numbers: 52.58.Hm,29.27.Eg,41.75.Ak

I. INTRODUCTION

Heavy ion fusion driver designs require in general, multiple intense ion beams with small spots and short durations to impinge on the target with precise timing. To generate the illumination pattern required by the target design, multiple drift compression beamlines with bends are usually required to transport beams from the multi-beam linear accelerators to the target. For two-sided or one-sided indirect target designs, the final focusing magnets for each beam subtend a finite solid angle and area near the entrance to the reactor chamber. Since there are many such beams, packing considerations force some beams to be aimed at the target at significant angles, for example at about 20 degrees, relative to the polar axis of the group of beams. Direct targets require spherically symmetric beam configurations, implying yet larger angles of incidence at chamber entrance.

The pulse length and focal spot sizes at target are fundamentally limited by beam emittances just before the focus. How the beam dynamics within the final compression beamline affect the final emittances therefore becomes a crucial question. In the presence of bends, the transverse dynamics is greatly affected by longitudinal momentum dispersion. One source of momentum spread comes from the head to tail velocity tilt required for beam compression, which will lead to centroid offset[1]. Another is the local velocity spread, which will also contribute to transverse emittance growth. Both the local velocity spread as well as head-to-tail distortion of the longitudinal phase space can lead to longitudinal emittance growth. Understanding the longitudinal emittance growth and finding ways of minimizing it, is the primary focus of this paper.

In this study, simulations are carried to understand the origin and parametric dependence of the emittance growth, using WARP, a 3-dimensional particle-in-cell code, which treat fields as electrostatic. The results are compared to an analytic model using an approximation to the problem of the longitudinal space charge self-field of an intense, long beam ("g-factor" model).[2,3,4]

II. SIMULATION PARAMETERS AND RESULTS ON FINAL BEAM DIMENSIONS

In this paper, we use an example of a direct target, because the requirement on spherical symmetry is more demanding on the drift compression beamline design. The example we consider is a 1MJ driver with 128 beams of 500MeV Rubidium+1 ions[5]. Beams are in a 4 polar ring configuration (Fig. 1). In a previous study, it was shown that this configuration could achieve sufficient uniformity for a direct target[6]. Because the beam channels are arranged in an annular symmetric configuration with beams entering from both sides, this essentially only requires 2 independent channel designs. In this study, we consider only the channel design for the smaller angle. Each channel consists of bends, a matching section, a plasma-filled neutralized drift[7] and final focusing section. The bending section of each channel is made of two arcs arranged in opposite directions, adding up to a net of about 37 degrees of bend. The bending dipoles are in combined-function magnets with the confining quadrupoles, each 0.8m long and the lattice period is 2m. After the bends end there is a matching section, which consists of the last four quadrupoles just before the start of neutralization. They change the beam envelope to circular and slightly diverging when it enter the neutralized drift, allowing the beam to expand before the final focusing magnets. The length of the neutralized drift is about 27m, in which the 12T final focus solenoid is placed at 4m before the target, close to the limit posed by typical chamber size and neutron induced damage. The total length of the whole compression section is about 91m, which is reasonable for cost and engineering issues. Table I lists some parameters used.

The effect of emittance on the final spot size and pulse length is shown by two main runs: one with canonical parameters as shown in Table I, and another with the same parameters, except for the initial emittances which are set to zero in all directions. The latter case corresponds to the most optimistic results for spot size and pulse length achievable under these conditions. The

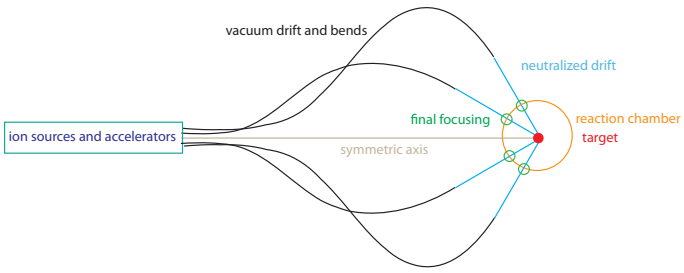

FIG. 1. Overview of beam channels geometry. The opposite side (which is not shown here) is identical.

TABLE I. Parameters used in this study

Parameter	Value
Initial peak current/beam (A)	100.0
Energy/beam (kJ)	7.5
Initial perveance	5.35×10^{-5}
Initial pulse length, r.m.s. (ns)	51
Initial transverse emittance (m rad)	5.2×10^{-5}
Initial longitudinal emittance (m rad)	4.56×10^{-3}
Velocity tilt	10%
Section total length (m)	91
Bend length (m)	20, 30
Neutralized drift length (m)	27
Lattice period (m)	2.0
Quad length (m)	0.8
Quad strength (T/m)	64.33
Max dipole strength (T)	4.65
Undepressed tune (degree)	72
Pipe radius (cm)	10

beam has semi-gaussian distribution and a parabolic current profile, loaded with matched envelope in the lattice and given a linear head-to-tail velocity tilt for compression.

We first consider canonical parameters. As the beam runs along the channel, its dimensions are recorded as function of z (Fig. 2, 3). In particular, at the focus around z=91m, the final pulse length (twice rms) is about 4.8 ns and the spot size is about 5 mm on the target. Next for the case with no initial emittance, the pulse length is 1.2 ns and a spot of roughly 2.6 mm, where ϵ_z and ϵ_x just before the focus are approximately 1.2×10^{-3} m rad and 3.5×10^{-5} m rad respectively. These values are minimum achievable with the set of parameter used. To understand the physical origin of this emittance growth, we vary the input parameters, and observe the parametric dependence of the growth rate. The findings will be discussed in the next sections.

The final focused spot size is roughly given by transverse emittance divided by the final focus angle provided

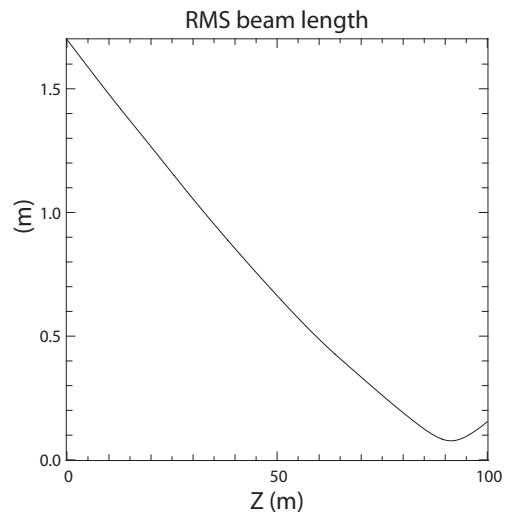

FIG. 2. Beam length as a function of z.

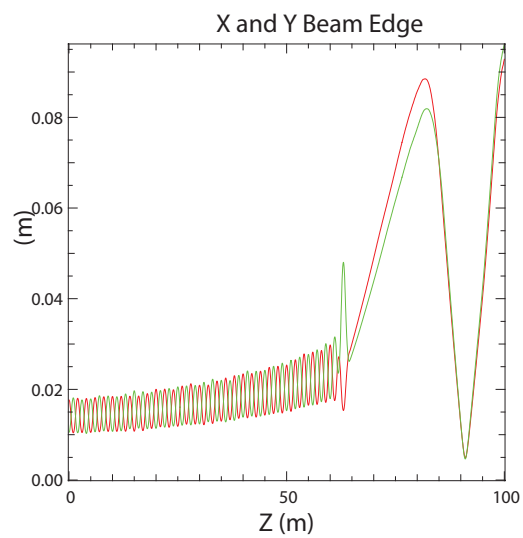

FIG. 3. Beam envelope (twice rms) as function of z. (red is x and green is y)

by final focus magnet a':

$$a_{final} \approx \frac{\epsilon_x}{|a'|} \tag{1}$$

Similar expression can be derived for the pulse length observing the similarities between transverse and longitudinal envelope equations in force-free region[8]. Here $|L'|$

is identified as beam velocity multiplied by final velocity tilt at the start of force-free region f:

$$L_{final} \approx \frac{\epsilon_z}{|L'|} = \frac{\epsilon_z}{v_b f} \tag{2}$$

In addition, possible contributing factors other than emittance to the final spot size are remaining centroid offset, chromatic effects from off-momentum slices and residual space charge effects. In the simulations, however, we observe those contributions from off-momentum slices are small. From Fig. 4 consider only the central slice (shown with blue line). Its spot is not much smaller than that of the whole beam, showing that the major limiting factor is still emittance.

III. EFFECT OF INITIAL EMITTANCE AND BENDS ON FINAL EMITTANCE

In reality, drift compression begins at the exit of accelerator, where the beams come out with non-zero emittance. In this section, the final emittance given a range of input transverse and longitudinal emittances, will be discussed. The final emittance is recorded at the end of bend section (z=60m), as we only focus on the growth within vacuum drift and bends, ignoring that in the matching and final focusing. Fig. 5 shows a sample simulation run of emittance as a function of distance travelled. The results of all runs are summarized in Fig. 6 and Fig. 7 respectively for cases with bends and just a straight channel of the same length.

The square of the longitudinal emittance is defined in general as:

$$\epsilon_z^2 = \frac{16}{v_b^2}(<(\Delta z)^2><(\Delta v_z)^2> - <\Delta z \Delta v_z>^2) \tag{3}$$

Here v_b is the average beam velocity, Δz and Δv_z are the position and velocity difference from their respective means.

In our simulation, the initial emittance is assumed to be purely thermal, with $\Delta v_z = \delta v_t$ which is uncorrelated with Δz ($<\delta v_t \Delta z = 0>$). The initial thermal emittance is then given by:

$$\epsilon_t^2 = \frac{16}{v_b^2} <(\Delta z)^2><\delta v_t^2> \tag{4}$$

We observed an emittance growth which arises from a new component δv_c which may or may not be correlated with Δz. The square of the emittance may then be written:

$$\epsilon_z^2 = \frac{16}{v_b^2}(<(\Delta z)^2><(\delta v_t + \delta v_c)^2> - <\Delta z(\delta v_t + \delta v_c)>^2) \tag{5}$$

$$\epsilon_z^2 = \frac{16}{v_b^2}(<(\Delta z)^2>(<\delta v_t^2> + <\delta v_c^2> + 2<\delta v_t \delta v_c>) - <\Delta z \delta v_t>^2 - <\Delta z \delta v_c>^2 - 2<\Delta z \delta v_t><\Delta z \delta v_c>) \tag{6}$$

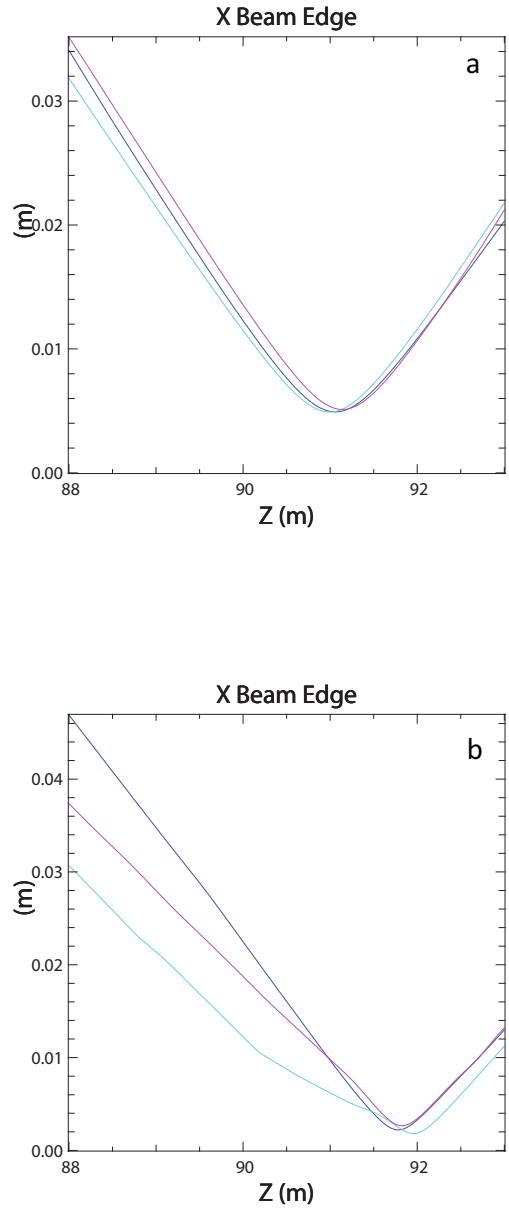

FIG. 4. Beam edge as function of z near the focus showing a small chromatic effect: blue line corresponds to central slice; purple and cyan lines are off momentum slices near the beam tail and head respectively. Two cases shown here are with normal emittance (a) and zero initial emittance (b).

Now if δv_c and δv_t are uncorrelated, i.e. $<\delta v_t \delta v_c> = 0$, then,

$$\epsilon_z^2 = \epsilon_t^2 + \epsilon_c^2 \tag{7}$$

Where $\epsilon_c^2 = \frac{16}{v_b^2}(<(\Delta z)^2><\delta v_c^2> - <\Delta z \delta v_c>^2)$ We

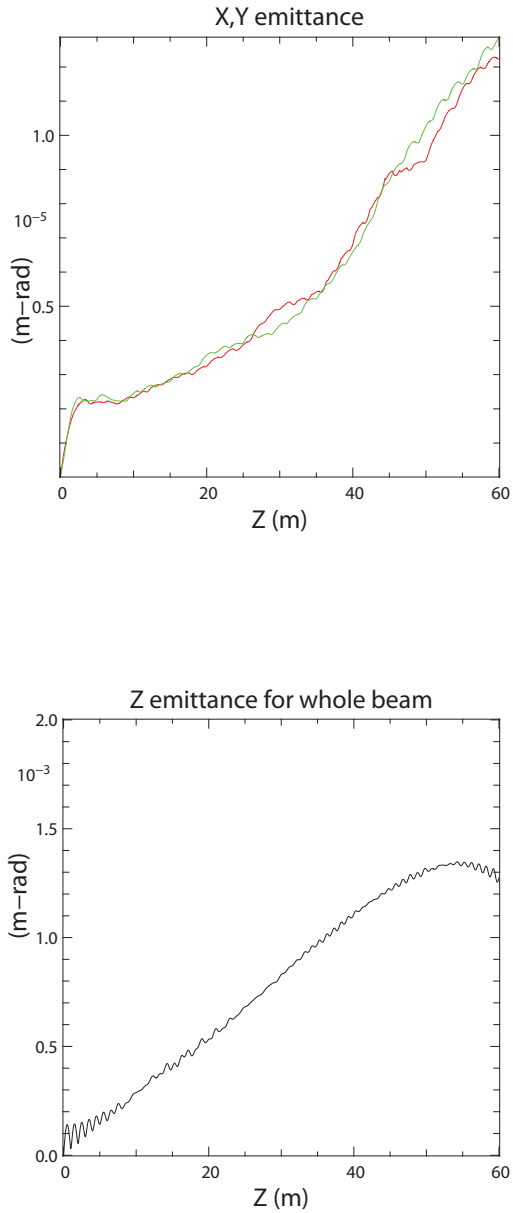

FIG. 5. One example of central slice x (red),y (green) emittances vs. z and whole beam z emittance vs. z, all emittance are initially zero.

define $\Delta\epsilon_z^2$ as the change in the square of the emittance,

$$\epsilon_{zf}^2 = \epsilon_{zi}^2 + \Delta\epsilon_z^2 \tag{8}$$

If the emittance growth and the assumed initial thermal spread are uncorrelated, then, as discussed above, we expect $\Delta\epsilon_z^2$ to be independent of the initial emittance ϵ_{zi}. Fig. 8 and Fig. 9 demonstrate that this is indeed the case. Indeed, $\Delta\epsilon_z^2$ is also independent of ϵ_{xi} and no matter if

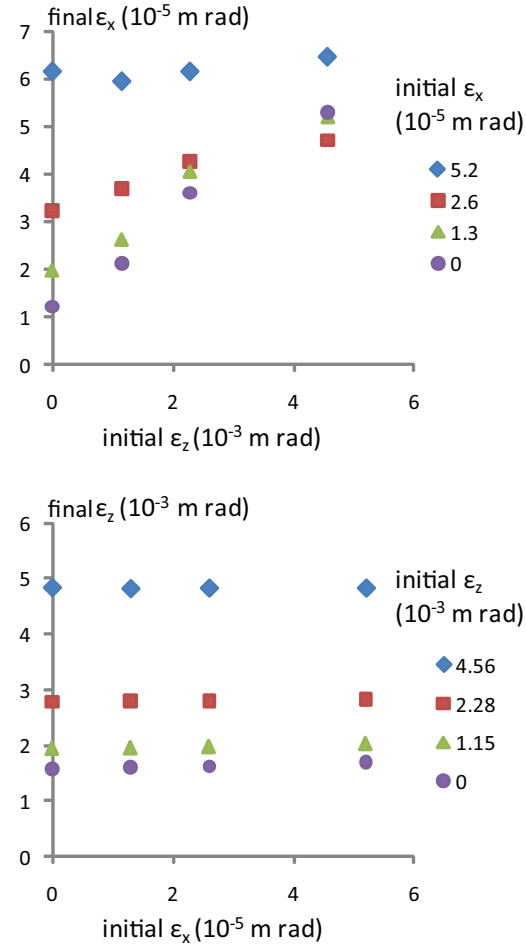

FIG. 6. Final emittance (x and z) vs. initial emittance (x and z)

bends are present.

On the other hand, if we treat transverse emittance similar to above, we observe $\Delta\epsilon_x^2$ depends on ϵ_{xi} and especially ϵ_{zi} when bends are present (Fig. 8). This means is $\Delta\epsilon_x^2$ correlated to the initial thermal distribution. However, the correlation is much weaker without bends (Fig. 9), suggests momentum dispersion is a possible mechanism of correlation as particles within a slice traveling at different curvatures through the bends corresponding to their longitudinal momentum (see ref.[1] and ref.[9]). Hence the thermal ϵ_{zi} directly affects $\Delta\epsilon_x^2$ in the direction of the bends.

The fact $\Delta\epsilon_z^2$ are essentially constant suggests it may be dominated by a single mechanism (in this case, the longitudinal space charge effect), which will be addressed in the next section.

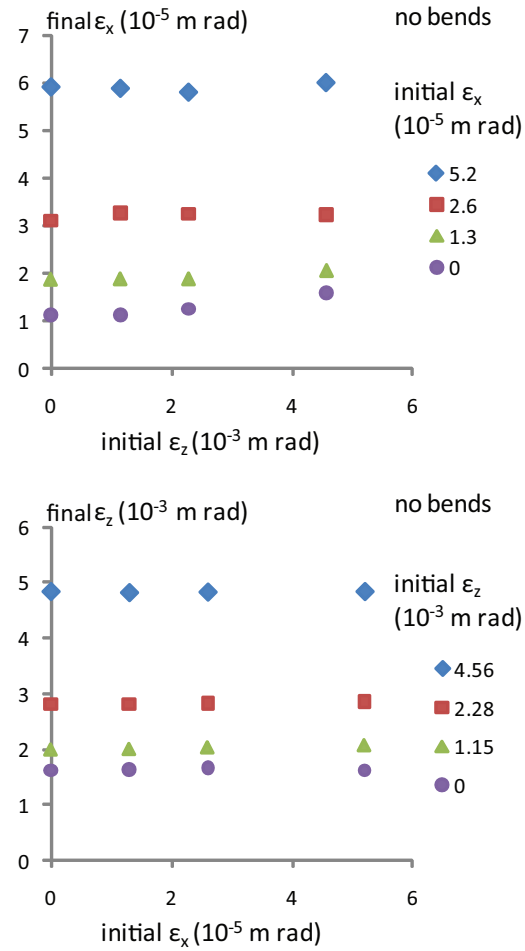

FIG. 7. Final emittance (x and z) vs. initial emittance (x and z), runs with bends removed.

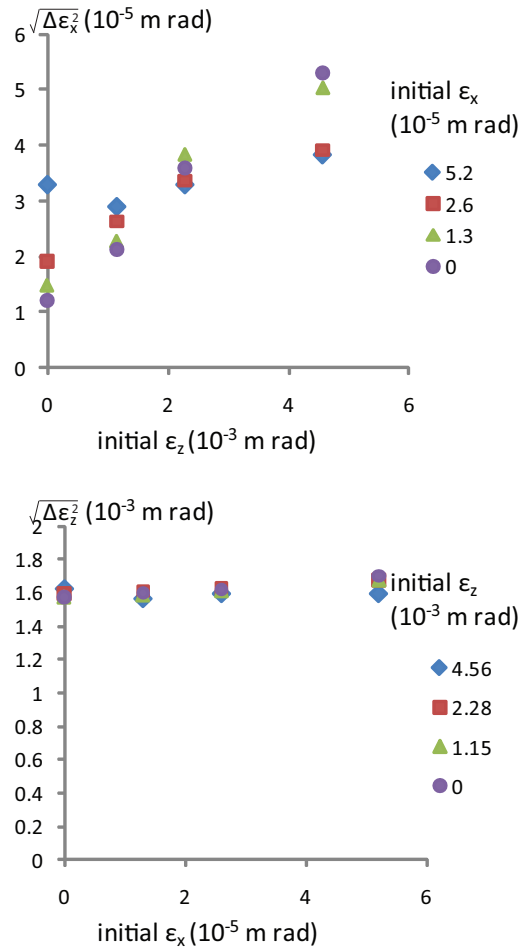

FIG. 8. Square root of $\Delta\epsilon_x^2$ and $\Delta\epsilon_z^2$ vs. initial ϵ_x and ϵ_z

IV. SPACE CHARGE EFFECT ON LONGITUDINAL EMITTANCE GROWTH

To understand the mechanism for longitudinal emittance growth in more detail, we carried out simulations of an initially cold beam with varying beam parameters. We consider a cold beam (i.e. zero emittance) as it provides the lower bounds for the final emittance and bunch length on target. In addition, previously presented results show the rate of longitudinal emittance growth is totally independent of the initial emittances assumed, thus it is sufficient to consider starting with zero emittance here. It provides an unambiguous scenario for the study of the physical mechanism for the emitance growth. Since we suspect that emittance growth is due to non-linear space charge effect, so the parameters we varied are related to the longitudinal space charge force. From the geometric factor model:

$$E_z = -\frac{g}{4\pi\varepsilon_o}\frac{\partial\lambda}{\partial z} \tag{9}$$

For an elliptical beam with radius independent of z and on axis:

$$g = \ln\left(\frac{R_p^2}{ab}\right) + 1 \tag{10}$$

where R_p denotes pipe radius, and a and b are envelope in x and y directions.

The parameters we vary include the geometric factor and peak current; these appear explicitly and scale directly with longitudinal electric force of the beam, In addition, we also vary the beam length and velocity tilt velocity tilt, both of which would affect the rate at which the beam compresses.

Starting with the canonical parameters: 100A current, 200ns pulse length and 10% velocity tilt, one parameter is varied each time. In all runs, longitudinal emittance growth follows the pattern exhibited in Fig. 8, which can be summarized as follow: an initial nearly linear growth followed by a slight acceleration in the growth rate and finally, the growth slows down, peaks at a certain value and drops back. Depending on the initial beam parame-

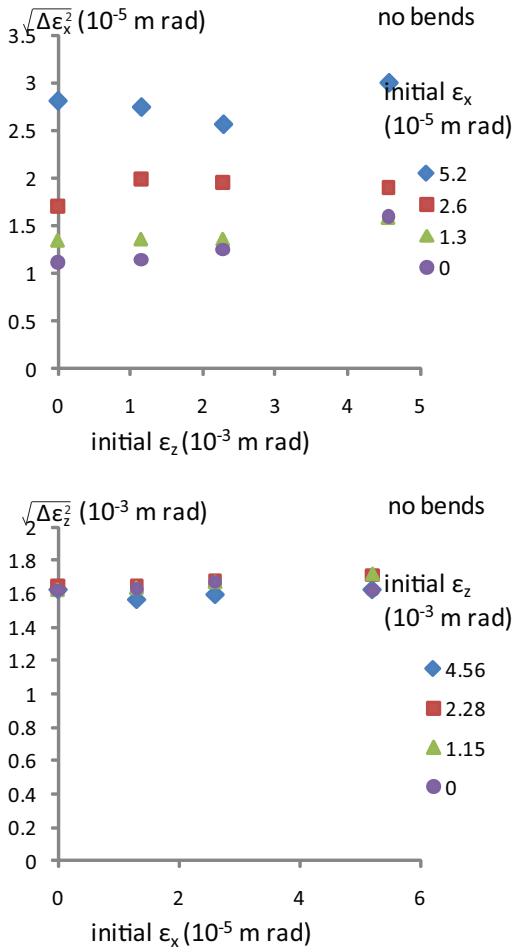

FIG. 9. Square root of $\Delta\epsilon_x^2$ and $\Delta\epsilon_z^2$ vs. initial ϵ_x and ϵ_z, runs with bends removed.

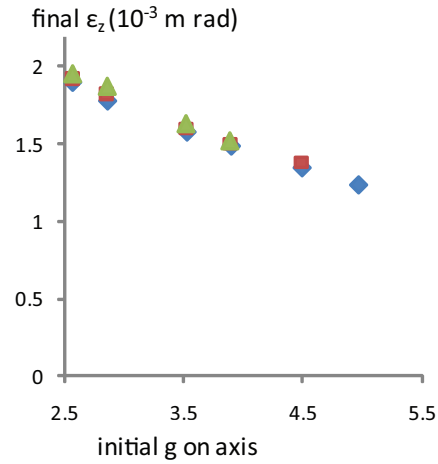

FIG. 10. Final z emittance at z=60m ($\times 10^{-}3$) vs. initial geometric factor on axis with various pipe radius.

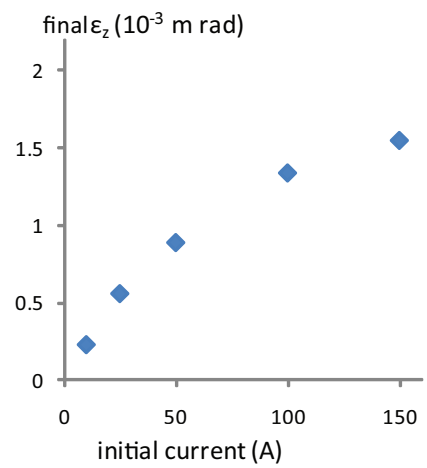

FIG. 11. Final z emittance at z=60m ($\times 10^{-}3$) vs. initial peak current.

ters, the relative position in z for the transition from the linear to nonlinear phase varies.

In Figures 10 to 13, we summarize the final emittance at the position of 60 m. In Fig. 10, we vary the geometric factor; this is done by changing the pipe radius (10cm, 8cm and 5cm) and/or the focusing strength to adjust the beam envelope. The observed dependence on g factor is due primarily to the varyng onset of the nonlinear phase and the associated final drop, larger g values corresponding to an earlier onset, and thus lower final emittance. In Fig. 11, we vary the initial beam current; it is varied together with focusing strength to keep the beam size approximately constant. Results show that the final emittance has a strong dependence on current, which is consistent with our expectation as space charge force increases linearly with current. In Fig. 12, we vary the initial beam length, while the peak current is kept constant. The total amount of charge is therefore changing with beam length. It is somewhat surprising that the growth is nearly independent of the beam length. For the shorter beams, the slightly lower final emittance is due to an earlier onset of the nonlinear phse, in contrast to the long beams which stay in the linear regime through the entire 60 meters. Lastly, we vary the amount of velocity tilt, and the result is shown in Fig. 13. We found small dependence of final emittance within the range tested.

In the above runs no bends were present. We have found that the effects of the bends are negligible in the high current cases. The effects of bends show up in cases with currents less than around 30A. (See Fig. 14)

Looking at the same data at an earlier position, (at z=20m), the growth is linear in all cases. At this position, the features noted become even more evident. The linear growth rate is clearly independent of g factor, pulse length, and velocity tilt, and is linear with current. This very simple result motivated us to look for an analytic understanding, which we present in the next section. The WARP data at 20m will be shown together with the an-

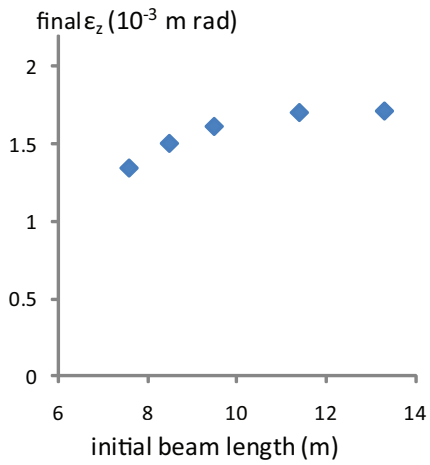

FIG. 12. Final z emittance at z=60m ($\times 10^-3$) vs. initial edge-to-edge beam length, with fixed peak current, thus total charge scales proportionally with beam length.

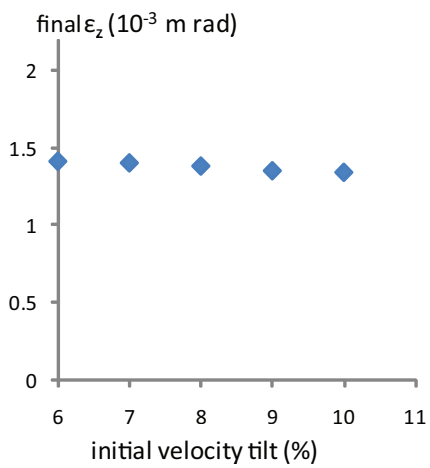

FIG. 13. Final z emittance at z=60m ($\times 10^-3$) vs. initial velocity tilt.

alytic results in Figures 16 to 19.

V. ANALYTIC RESULT ON LONGITUDINAL EMITTANCE GROWTH

In this section, we calculate the linear growth rate within the g-factor model. We assume a perfect parabolic line charge density and a linear initial phase space which has zero emittance. Although realistic beams have non-zero emittance, we will focus on the zero emittance case. The reason is same as that in doing simulations, since it is for a baseline study. In addition, the same emittance can be obtained from many individual phase space profiles, each canbehave differently. There is in general no unique solution in the case with non-zero initial emittance, so we stick with zero emittance, which phase space can only be straight lines. In sections below, we consider 2 ideal cases: the first case for a beam with constant beam radius from head to tail, and a second case with uniform current density throughout the entire beam. We calculate the contribution to longitudinal emittance by the non linear terms in g, by directly evaluating the terms from the definition of longitudinal emittance (Equation 3). The ensemble average terms are calculated directly by integration, for example:

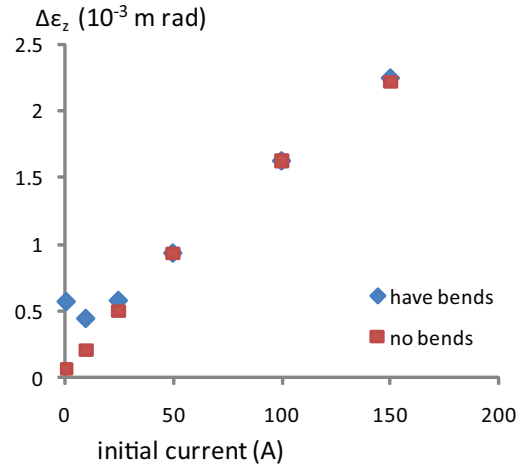

FIG. 14. z emittance growth as a function of initial current with non-zero initial emittance, effect of bend shows up in low current regime. Otherwise, longitudinal emittance growth is dominated by space charge.

$$\left\langle (\Delta v_z)^2 \right\rangle = \frac{1}{C} \int \rho (v - v_b)^2 d^3 r \tag{11}$$

C is the total charge and ρ is the volume charge density, the beam extends from $z = -L/2$ to $+L/2$. The beam starts with a perfectly linear velocity tilt with zero longitudinal emperature, i.e. zero initial longitudinal emittance.

A. Beam with uniform radius

Consider a circular beam with uniform radius along its length, with uniform cross sectional density and parabolic line density, i.e.

$$\rho(z) = \frac{\lambda(z)}{\pi a^2} \tag{12}$$

$$\lambda(z) = \frac{3C}{2L}(1 - 4\frac{z^2}{L^2}) \tag{13}$$

Staying on axis, the longitudinal space charge force is linear. However, there is a radial dependence of g:

$$g(r) = 2\ln(\frac{R_p}{a}) + 1 - \frac{r^2}{a^2} \tag{14}$$

hence the electric field:

$$E_z(z,r,t) = \frac{g(r)}{4\pi\varepsilon_o} \cdot 12C\frac{z}{L^3} \tag{15}$$

which leads to off axis particles experiencing smaller forces than those on axis. If particles always stay at same distance from axis, i.e. flow is laminar, there will be a systematic difference in force within each beam slices, which would lead to a spread in beam energy. The time dependence is hidden in L, as the beam we consider is compressing due to the given tilt. Here we take some simplifications to the problem. First, we assume the beam maintain a self similar shape (i.e. parabolic), only its length L scales with time, hence the position parameter is $s = z/L$ rather than z. Second, within the short time interval, we assume z is not affected by E_z, by the fact that z scales with $E_z t^2$, its effect appears slower than v_z. This is also required to be consistent with the first assumption. Therefore $\langle(\Delta z)^2\rangle$ is just the mean-square length:

$$\langle(\Delta z)^2\rangle = \frac{1}{C}\int \rho z^2 d^3r = \frac{L^2}{20} \tag{16}$$

The third assumption is we neglect the space charge slowdown effect on beam compression, i.e. beam length only depends on the initially given tilt. In other words, beam length change linearly with time, such that:

$$L(t) = L_o - v_b f t \tag{17}$$

where L_o is the initial length and f is the initial tilt. This approximation is quite good within a short time, especially if the tilt is large.

With all these assumptions, we can now evaluate the evolution of emittance:

$$v(r,s,t) = v_b(1+sf) + \frac{12qCg(r)}{4\pi\varepsilon_o m} s \cdot F(t) \tag{18}$$

with

$$F(t) = \int \frac{dt'}{(L_o - v_b f t')^2} = \frac{t}{L(t)\cdot L_o} \tag{19}$$

From velocity of particles,

$$\langle(\Delta v_z)^2\rangle = \frac{1}{C}\int \rho(v-v_b)^2 d^3r \tag{20}$$

$$= \frac{1}{C}\int \frac{3C}{2L\pi a^2}(1-4s^2)[v_b sf + 12ACg(r)sF(t)]^2 d^3r \tag{21}$$

$$= \frac{12}{5}(ACF)^2(1-3g_o-3g_o^2) + \frac{3}{5}ACF(2g_o-1)v_b f + \frac{v_b^2 f^2}{20} \tag{22}$$

where $A = q/4\pi\varepsilon_o m$ and $g_o = 2\ln(R_p/a)+1$

Similarly,

$$\langle(\Delta v_z z)\rangle = \frac{1}{C}\int \rho z(v-v_b) d^3r \tag{23}$$

$$= \frac{L}{C}\int \frac{3C}{2L\pi a^2}(1-4s^2)[v_b sf + 12ACg(r)sF(t)]s d^3r \tag{24}$$

$$= [\frac{3}{10}ACF(2g_o-1) + \frac{v_b f}{20}]L \tag{25}$$

Putting all terms together:

$$\epsilon_z^2 = \frac{16}{v_b^2}[\langle(\Delta z)^2\rangle\langle(\Delta v_z)^2\rangle - \langle\Delta z\Delta v_z\rangle^2] \tag{26}$$

$$= \frac{144}{300 v_b^2}(\frac{AC}{L_o}t)^2 \tag{27}$$

Hence

$$\epsilon_z = \sqrt{\frac{12}{25}}\frac{qC}{4\pi\epsilon_o m v_b L_o} t \tag{28}$$

or

$$\epsilon_z = \sqrt{\frac{12}{25}}\frac{q^2 N}{4\pi\epsilon_o m v_b^3 \tau_o} d \cong 0.69\frac{q^2 N}{4\pi\epsilon_o m v_b^3 \tau_o} d \tag{29}$$

Where N is number of ions, d is the distance travelled and τ_o is the initial pulse duration in time. We note that the longitudinal emittance only depends on total charge/initial beam length, which is also proportional to the peak line charge density. The growth is linear with time (or distance travelled), i.e. a constant growth rate. These features agree with the simulation results from Section 4.

It is interesting that the emittance growth does not depend on the vacuum chamber radius and beam radius, since the space-charge force clearly depends on these parameters (evident from the g-factor model). The physical origin can be traced back to Eq. (10), where the leading term in the g-factor depends on the chamber and beam radius, but the nonlinear term, which is responsible for the emittance growth, depends only on the dimensionless parameter r/a.

B. Beam with uniform charge density

Another ideal case is a beam with uniform charge density all over its volume. This is in fact the initial condition assumed for the beams in the simulations of Section 4. For the same parabolic line density and cross section:

$$\rho = \frac{\lambda(z)}{\pi a^2(z)} \tag{30}$$

$$\lambda(z) = \frac{3C}{2L}(1-4\frac{z^2}{L^2}) \tag{31}$$

The beam envelope can be written as a function of $s = z/L$:

$$a^2(z) = \frac{3C}{2\pi\rho L}(1-4s^2) \tag{32}$$

We assume g factor still holds towards the ends of beam, which is given by:

$$g(s) = 2\ln(\frac{R_p}{a}) = \ln(\frac{2\pi\rho L R_p^2}{3C(1-4s^2)}) \tag{33}$$

Note that this assumption may not be really correct and that divergence occurs as s tends to $\pm 1/2$. However as the line charge density falls off rapidly, the final result converges. As the edge contribution is small, we expect emittance calculated is well approximated.

In Eq. (29), the g factor consists of only axial dependence, as the radial term is cancelled exactly in below expression, since ρ and hence λ/a^2 is constant[10]:

$$E_z = -\frac{1}{2\pi\epsilon_o}[\frac{1}{2}(1-\frac{r^2}{a^2})+\ln(\frac{R_p}{a})]\frac{\partial\lambda}{\partial z} - \frac{1}{2\pi\epsilon_o}(1-\frac{r^2}{a^2})\frac{\lambda}{a}\frac{\partial a}{\partial z} \tag{34}$$

Where

$$\frac{\partial a}{\partial z} = \frac{a}{2\lambda}\frac{\partial\lambda}{\partial z} \tag{35}$$

Following similar calculations as above, but replacing $g(r)$ with $g(s)$:

$$\langle(\Delta v_z)^2\rangle = \frac{1}{C}\int \rho(v-v_b)^2 d^3r \tag{36}$$

$$= \frac{4}{125}(ACF)^2(1772-75\pi^2+930g'+225g'^2)+\frac{2}{25}ACF(15g'+31)v_b f+\frac{v_b^2 f^2}{20} \tag{37}$$

where

$$g' = \ln(\frac{R_p^2}{4a_o^2}) = 2\ln(\frac{R_p}{2a_o}) \tag{38}$$

$$a_o^2 = \frac{3C}{2\pi\rho L} \tag{39}$$

Similarly:

$$\langle(\Delta v_z z)\rangle = \frac{1}{C}\int \rho z(v-v_b)d^3r \tag{40}$$

$$= [\frac{1}{25}ACF(15g'+31)+\frac{v_b f}{20}]L \tag{41}$$

The final result is

$$\epsilon_z = \frac{4}{25}\sqrt{811-75\pi^2}\frac{qC}{4\pi\epsilon_o m v_b L_o}t \tag{42}$$

or

$$\epsilon_z = \frac{4}{25}\sqrt{811-75\pi^2}\frac{q^2N}{4\pi\epsilon_o m v_b^3\tau_o}d \cong 1.35\frac{q^2N}{4\pi\epsilon_o m v_b^3\tau_o}d \tag{43}$$

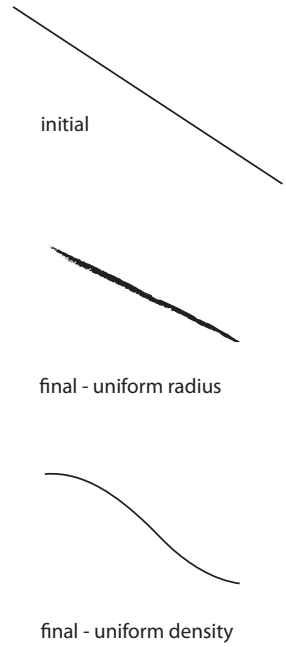

FIG. 15. Longitudinal phase space (v_z vs. z) evolution for the ideal cases. Top - initial phase space for both two cases, with linear tilt and no temperature. Middle - uniform radius case showing increase in thickness of the phase space as a growth of temperature. Bottom - uniform density case showing a head-to-tail distortion (S-ing) results in a growth of effective area.

The formula has the same form as the previous case with uniform envelope with just a different numerical constant. Both cases show the same dependence of longitudinal emittance growth on the initial line charge density only. We observe that the emittance growth in Case A corresponds to a growth of local temperature, while Case B results from a nonlinear distortion of head-to-tail beam profile. In case B, the phase space is still a thin line with no area, so the area is not directly related to emittance like common understanding (as that in case A). It seems the rms definition of emittance here does not accurately reflect thermal spread in velocity. However, the distorted beam will not converge to a single point on the target although it has no occupied phase space area. So the rms emittance rather than the phase space area is ultimately the parameter that is directly related to the pulse length at target. Fig. 15 is a schematic illustration of the evolution of the longitudinal phase spaces in these two ideal cases.

C. Comparison of analytic formula with warp simulation

We take the warp simulation results and compare with the derived formula, the longitudinal emittance values at z=20m are plotted as functions of initial parameters (Fig. 16, 17, 18, 19). The derived and simulated growth with canonical parameters is plotted as a function of dis-

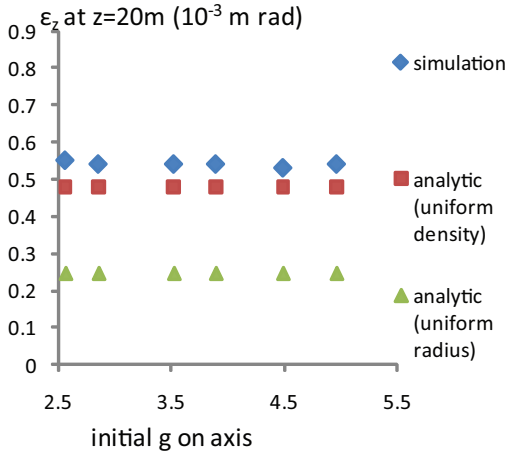

FIG. 16. z emittance at z=20m ($\times 10^-3$) vs. initial geometric factor on axis, showing 2 cases with uniform beam radius (red), uniform charge density (green) and warp simulation (blue).

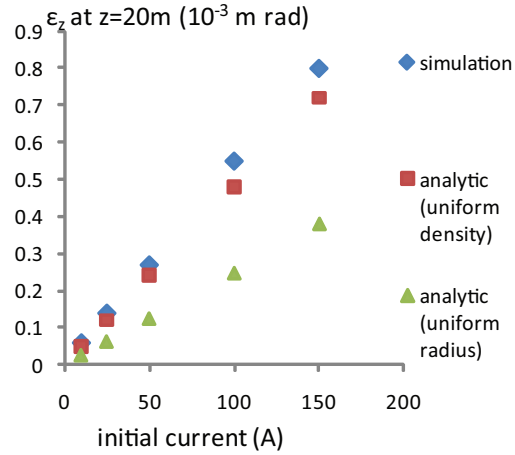

FIG. 17. z emittance at z=20m ($\times 10^-3$) vs. initial current, showing 2 cases with uniform beam radius (green), uniform charge density (red) and warp simulation (blue).

tance as well (Fig. 20). Both results show that initial growth rate of ϵ_z is proportional to initial current but independent of the other 3 parameters. The prediction of the uniform charge density case is well matched to the simulations in terms of the initial growth rate, except for the ripples related to quadrupole focusing. This is expected as the beam in the WARP simulation is initialized with the assumptions of Case B. For more general beams intermediate between the cases considered above, it is expected that both axial and radial non-linearities will appear, and the final result will also have same form as above, with different numerical factors depending on details of the initial beam profile. We can write a more general formula as:

$$\epsilon_z = k \frac{q^2 N}{4\pi\epsilon_o m v_b^3 \tau_o} d \tag{44}$$

Here k is the numerical factor to be determined. For the two cases discussed above, k has values of order unity.

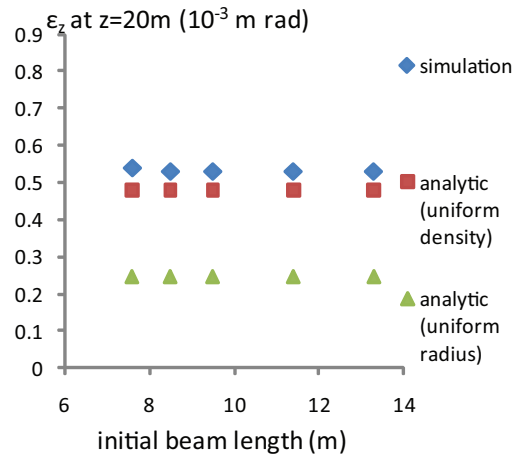

FIG. 18. z emittance at z=20m ($\times 10^-3$) vs. initial beam length with fixed peak current, showing 2 cases with uniform beam radius (green), uniform charge density (red) and warp simulation (blue).

VI. CONCLUSIONS

Longitudinal emittance is a limiting factor to the final pulse length. In many driver designs where bends are present, it also induces transverse emittance growth and in turn enlarges the spot size on target. Both of them are crucial requirements in heavy ion fusion applications. We present in this paper one mechanism for longitudinal emittance growth, due to self non-inear space charge force. The growth is proportional to line charge density and distance travelled. It suggests that the growth can be reduced by designing beamlines with short drift distance and separating high current beams into multiple beamlets, when short pulses are required. Another important question is whether the emittance growth described in this paper can be reversed or mitigated, either by external means or by inherent mechanisms. We observe that in the case of uniform charge density (case B), the emittance growth mainly results from a head-to-tail distortion of the longitudinal phase space (it takes an "S" shape). This emittance can be reduced if the distortion is corrected, for example, by correction voltage pulses with just the right form to undo the S-ing, This method becomes prohibitively costly if applied to individual beams in each of the drift compression beamlines, where they are separated. A second possible way is to prepare the beam bundle before the exit of the accelerator with a head-to-tail energy profile to compensate in advance the

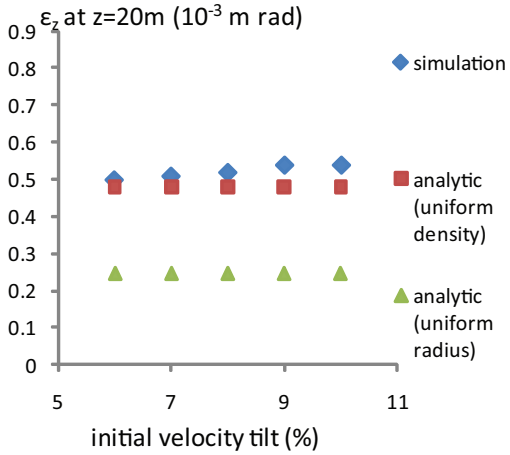

FIG. 19. z emittance at z=20m ($\times 10^{-}3$) vs. initial tilt, showing 2 cases with uniform beam radius (green), uniform charge density (red) and warp simulation (blue).

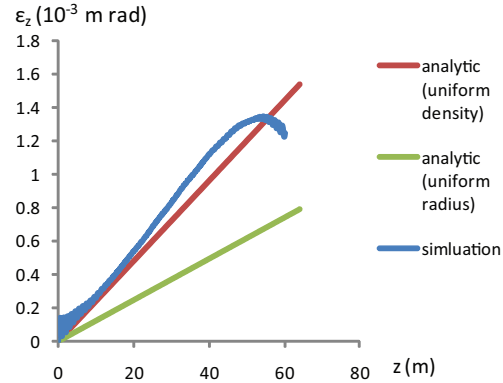

FIG. 20. z emittance vs. z (m), showing 2 cases with uniform beam radius (green), uniform charge density (red) and warp simulation (blue).

nonlinear distortion in the drift compression section. Finally, we observed in our simulations a significant drop in the longitudinal emittance as we move beyond the region of linear growth. We observe that the phase space distortions undo itself to a certain extent .We are exploring all of these mechanisms for the reduction of longitudinal emittance.

[1]E. P. Lee and J. J. Barnard, "Bends and momentum dispersion during final compression in heavy ion fusion drivers." Laser and Particle Beams **20**, 581–584 (2002).

[2]W. M. Sharp, A. Friedman, and D. P. Grote, "Effects of longitudinal space charge in beams for heavy-ion fusion." Fusion Engineering and Design **32–33**, 201–208 (1996).

[3]S. Koscielniak, "Longitudinal space-charge geometric factor for an elliptical beam." in *Proceedings of the 2001 Particle Accelerator Conference* (2001) pp. 2970–2972.

[4]R. Baartman, "Form factor g in longitudinal space charge impedance." (1992).

[5]Y. Y. Lau, S. S. Yu, J. J. Barnard, and P. A. Seidl, "Final compression beamline systems for heavy ion fusion drivers." (2010), Laser and Particle Beams (submitted).

[6]J. Runge and B. G. Logan, "Nonuniformity for rotated beam illumination in directly driven heavy-ion fusion." Physics of Plasmas **16**, 033109 (2009).

[7]P. K. Roy, S. S. Yu, E. Henestroza, A. Anders, F. M. Bieniosek, J. Coleman, S. Eylon, W. G. Greenway, M. Leitner, B. G. Logan, W. L. Waldron, D. R. Welch, C. Thoma, A. B. Sefkow, E. P. Gilson, P. C. Efthimion, and R. C. Davidson, "Drift compression of an intense neutralized ion beam." Physical Review Letters **95**, 234801 (2005).

[8]D. Neuffer, "Extensions of the longitudinal envelope equation," Tech. Rep. (Fermi National Accelerator Lab, 1997).

[9]J. J. Barnard, H. D. Shay, S. S. Yu, A. Friedman, and D. P. Grote, "Emittance growth in heavy ion recirculators," in *Proceedings of the 1992 Linear Accelerator Conference* (1992).

[10]J. J. Barnard and K. Horioka, "Induction accelerators," (Springer Berlin Heidelberg, 2011) Chap. 9.

Prepared by LLNL under Contract DE-AC52-07NA27344